Indian J. Phys. **78A** (1), 19-25 (2004)

Nanomaterials–2003

INTERNATIONAL JOURNAL

IJP

Porous silicon a natural nano structure for sensing and photonic applications

H Saha*, S M Hossain and J Das#

IC Design and Fabrication Centre, Department of Electronics and Telecommunication Engineering
Jadavpur University, Kolkata-700 032, India

E-mail : juiec@vsnl.com

Abstract : Porous silicon (PS) is emerging as an important nanocrystalline material that can be formed and controlled suitably for application as gas and vapour sensors, as well as LEDs and photonic crystals. In this paper, results of in-depth investigations on the role of formation parameters on porosity, layer thickness and the extent of non-directional pore growth in PS have been reported. Measurements like SEM and AFM techniques, photoluminescence and XRD studies, have been performed to get the dimensions of Si-nano-crystallites and pores. IR absorption spectra have been employed to identify the chemical species in as-grown and aged PS layer. The luminescence property of PS has been used to fabricate a 7-segment display. A theoretical model for vapour sensing in nano-porous medium has been outlined and implemented in porous silicon vapour sensor.

Keywords : Porous silicon, nano-structure, luminescence, sensor.

PACS Nos. : 78.67.Bf, 81.07.-b, 61.10.Nz, 07.07.Df

1. Introduction

Porous silicon has been discovered in 1956 by Uhlir [1] while performing electro-polishing experiments on silicon wafers using an HF based electrolyte. At that time it was not recognized as porous silicon. After the demonstration of tunable, efficient, visible and room temperature photoluminescence (PL) from PS in 1990 [2] and its possible explanation by quantum confinement of electrons and holes inside Si-nanocrystallites, it has got tremendous scientific and technological attraction throughout the last decade of the last century. Its optical [3], opto-electronic [4], mechanical [5], photovoltaic [6] and many other properties have been researched extensively.

In this paper we demonstrate our studies on the possibilities of modulating the nanostructures of porous silicon by controlling its formation parameters and thereby investigating the influence of this variation in nano crystalline morphology on its sensing and photonic applications.

2. Experimental

To study the structural morphology and opto-electronic properties of PS a number of samples have been prepared by electrochemical technique [7]. PS samples were formed on 1–2 Ω cm resistivity p-type (100) orientation c-Si wafers by anodization in HF-CH_3OH solution in a teflon bath with special electrode geometry [8]. Varying electrolyte concentration, formation current density and duration of etching has produced widely varied PS structures.

Porosity, layer thickness and uniformity factor [7], (a measure of pore branching in PS) has been measured using gravimetric method [9]. SEM and AFM micrographs have been obtained to get some direct idea about the PS top surface and morphology.

To study the possible changes that might occur at the surface of PS films due to washing de-ionised (DI) water and exposing to ambient air, IR transmission spectra were recorded. For this experiment, PS films were lifted off and mixed with KBr to prepare pellet for IR spectroscopy (Perkin- Elmer 597).

PL and XRD studies have been applied to get some information about the band structure and particle size of PS layer. PL spectra of the samples after washing in DI water followed by exposure to ambient air have been recorded by an ORIEL set up under UV excitation of 350 nm. From PL peak energy values, particle size has been calculated using the PS band structure proposed by Wolkin *et al* [10] for oxidized PS layer.

*Corresponding Author

#Permanent address : Department of Physics, Gokhale Memorial Girls College, Kolkata-700 020, India

XRD measurement has been performed on the PS samples and the diffraction data have been obtained using powder diffractometer (Bruker D8 Advance). Si-particle size has been calculated from the peak broadening using Scherrer equation [11] given by

$$a = \frac{0.9\lambda}{B\cos\theta} \quad (1)$$

where B is the FWHM of the peak at θ.

To investigate the electrical properties of PS, dc conductivity of a number of PS samples has been measured. From this study, thick Al of 500 nm has been evaporated on the PS layers followed by heat treatment at 500°C for 45 sec to get ohmic contact [12].

3. Results

Figure 1 shows the SEM micrographs of top and cross-sectional view of a typical PS layer formed on p-Si. These figures clearly show the growth of pores in vertical as well as horizontal directions.

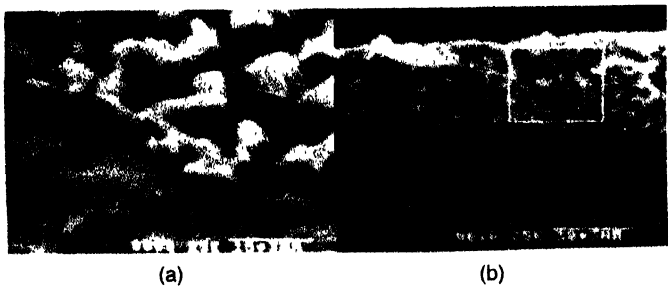

(a) (b)

Figure 1. SEM micrographs of a . top surface and b cross section of a PS layer having porosity ~70%

Figure 2 (i), (ii) and (iii) depict the variation of porosity layer thickness and uniformity factor with HF concentration in the electrolyte, formation current density and formation time respectively. Porosity and layer thickness of the samples have been found to vary between 40 to 85% and 1 to 6 μm respectively for the variation of formation parameters in the range mentioned in the figures. Uniformity factor which is a measure of vertical pore growth lies between 2 to 7% indicating large extent of pore branching in these PS layers formed on 1–2 Ω cm p-Si wafer.

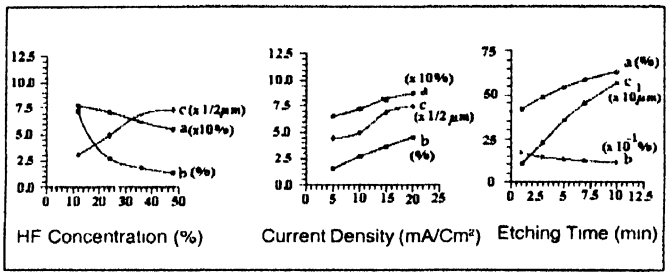

Figure 2. Variation of (a) porosity, (b) uniformity factor and (c) layer thickness with formation parameters of PS

Figure 3 shows AFM topographs and surface profile of two different PS layers. The PS layer formed with lower current density and hence lower porosity shows larger pores (~100 nm) than that formed with higher current density(~10 nm). However, density of pores is higher in the later case.

IR transmittance spectra of the PS layers in as-prepared (not washed in DI water) and water treated conditions are shown in curves (a) and (b) of Figure 4 respectively. IR study of as-prepared PS samples showed the lines at ~910, 740 and 630 cm^{-1} indicating the presence of different SiH_x on PS surface. This also showed the presence of broad lines at 2100 cm^{-1} indicating the presence of Si-H bonds where the Si-atom is back bonded to another Si-atom. The samples, which were washed in deionised water showed intense peak at 1070 cm^{-1} indicating the formation of Si-O-Si bond. The Si-H peak at 2100 cm^{-1} showed a simultaneous decrease. These curves clearly indicate growth

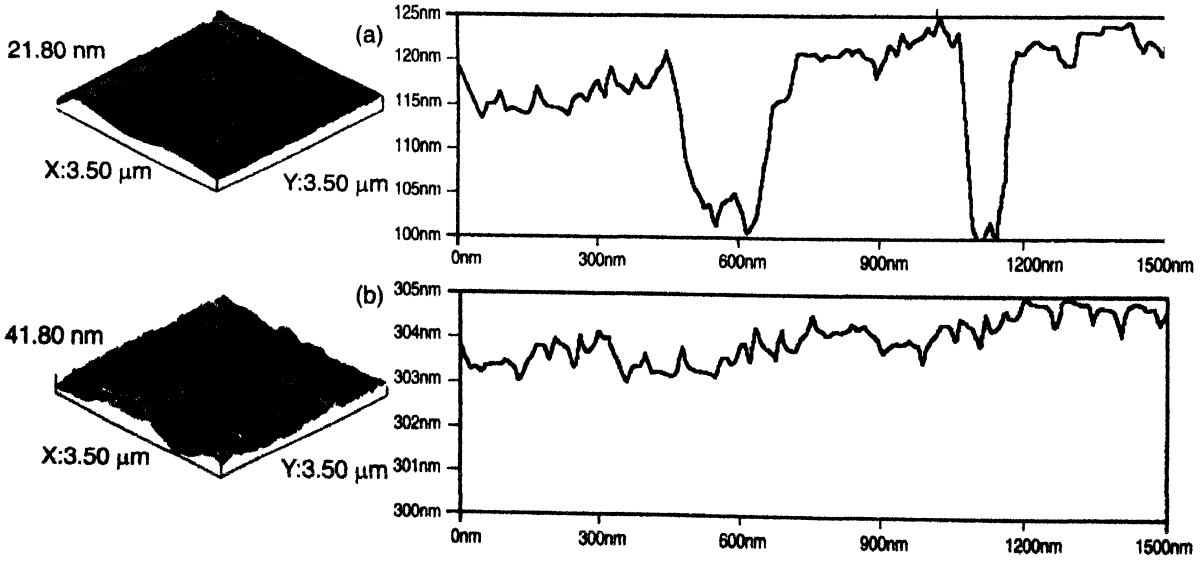

Figure 3. AFM topographs and surface profile of two different PS layers formed with 24% HF for 1 min using (a) 5 and (b) 20 mA/cm².

of oxide in PS layer after washing in water followed by exposure to ambient air. Growth of oxide further reduces the dimension of silicon nanocrystallites enhancing quantum confinement.

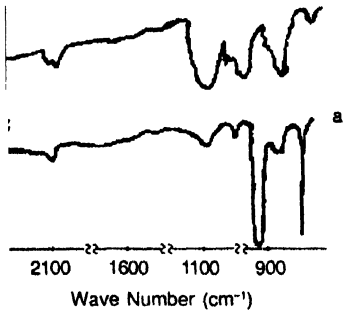

Figure 4. IR transmittance spectra of PS layers, (a) as anodized and (b) washed in DI water.

Figure 5a shows a photograph of a PL emitting PS layer in the red-orange region. PL spectra of some PS films formed with different current density in the range of 2–150 mA/cm^2 are shown in Figure 5b. For the samples prepared with 20 mA/cm^2 or more, double peak has been found. One of these peaks is at ~730 nm and independent of formation current density and the other

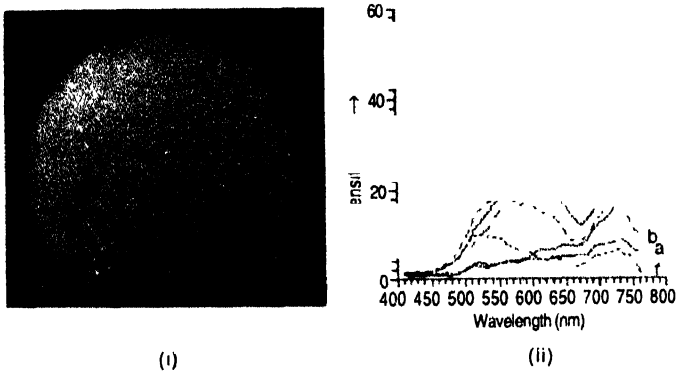

Figure 5. (i) Photograph of PL emission from PS, (ii) PL spectra of PS formed with 24% HF for 10 min using (a) 2, (b) 10, (c) 20, (d) 40, (e) 80 and (f)150 mA/cm^2

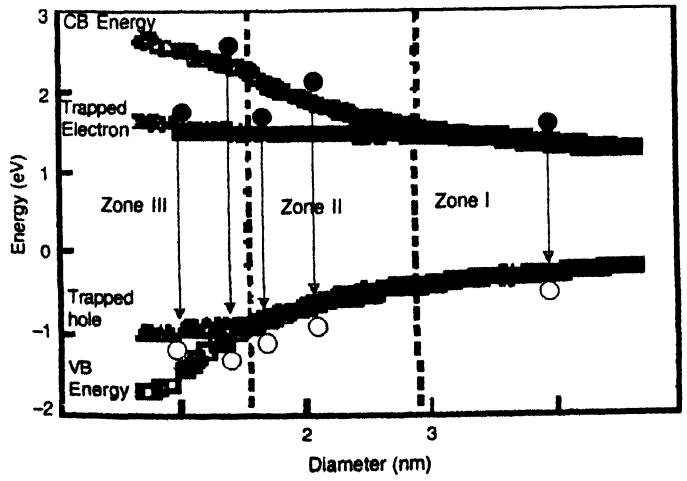

Figure 6. Band structure of oxidized PS layer as proposed by Wolkin *et al* [10] and the probable recombination mechanisms.

peak has been found to vary from 735 to 545 nm in this current density range. These results are in conformity with the band-model (Figure 6) of oxidized PS proposed by Wolkin *et al* [10]. Using this band model, particle size in PS layers are calculated from the PL energy of the peak blue shifting with formation current density using the following equation,

$$a = \left(\frac{c}{E_p - E_t} \right)^{1/n} \tag{2}$$

Here c and n are constants depending on the degree of confinement and having values 1.71 unit and 1.3 respectively for quantum dots. Values of calculated Si-particle size fall in the range of 2 to 10 nm and are shown in Table 1.

Table 1. Variation of PL peak wavelength and calculated Si-nanocrystal size in PS with formation current density.

J (mA/cm^2)	λ_{p1} (nm)	E_{p1} (eV)	λ_{p2} (nm)	Si particle size (nm)
2	735	1.687	—	9.88
10	700	1.771	—	5.88
20	637	1.947	729	3.41
40	597	2.077	731	2.67
80	567	2.187	731	2.28
150	545	2.275	729	2.04

Calculated values of Si-particle size for a typical PS sample from XRD powder diffraction (Figure 7) study also fall in the range of nanometer (3–10 nm).

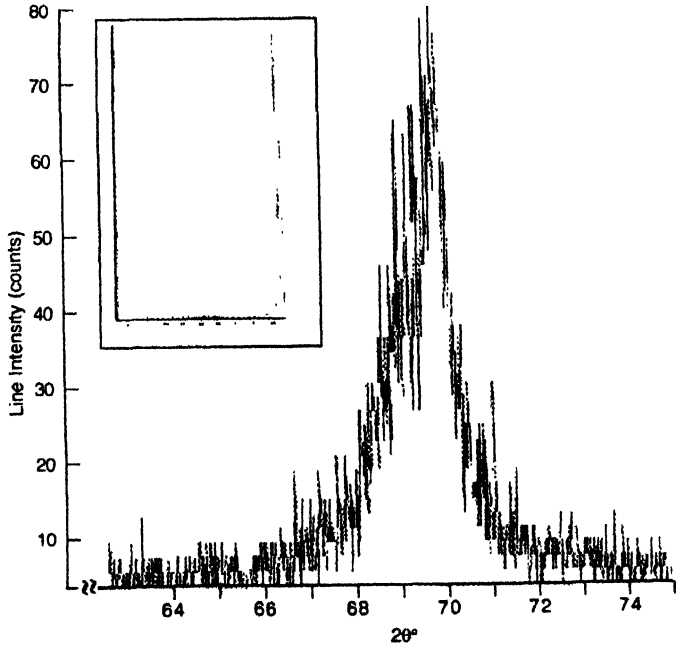

Figure 7. XRD diffraction peak for a typical PS Layer; Inset : The same for c-Si substrate.

Table 2 shows the experimentally found values of the effective conductivity. The conductivity decreases from 3.0×10^{-4} to 5.0×10^{-6} mho/cm for the variation of porosity in the range of 40 to 85 %.

Table 2. Variation of porosity and effective conductivity of PS layer with formation parameters

Formation parameters			P_m (%)	σ_{eff} (10^{-5}) (exp)
C (%)	J (mA/cm^2)	T (min)		
48	10	1	41.0	29 4
48	10	3	49.0	16 3
48	10	5	54 0	11 6
48	10	7	59 0	10 7
48	10	10	63 0	2 27
24	5	5	65.0	1.10
24	10	5	71 0	0 99
24	15	5	81.0	0.80
24	20	5	86 0	0 60
36	10	5	62 0	6 98
12	10	5	77.0	0.50

4. Discussion

From the experimental results obtained from SEM/AFM and gravimetric measurements, one can say that the porosity, layer thickness, pore size and pore morphology as well as pore density can be controlled over a wide range through the formation parameters. The AFM results (Figure 3) we have found depict that the average size of the pores varies from hundreds of nanometer to the order of a few nanometer. A distribution of pore size around the average value can be observed in each case. Low value of the uniformity factor indicates non-vertical branched pore growth. This also means existence of a distribution of pore dimension in PS. However, vertically grown uniform pores can also be developed in n-type c-Si using photolithography [14].

PL and XRD studies show that the Si-particle size in PS is in the nanometric scale leading to efficient light emission in the visible region primarily through quantum confinement [10,15]. The large value of spectral width of PL can be attributed to a normal distribution [16] of crystallite size around an average value. However, well defined PS column structure can also be developed using successive etching technique [17].

IR studies reveal the presence of silicon oxide in PS layers exposed in ambient air. So, PS can be modeled as a three-phase mixture [18] of voids and Si nano-particles embedded in amorphous silicon oxide (Figure 8). Dimension of each phase has a normal distribution around the average value that can be controlled through the formation parameters or by controlled oxidation [15].

Conductivity measurements show that change in the porosity can also vary the conductivity of this nano-composite. A comparison between the experimental conductivity and that calculated using GEMA [19] is shown in Figure 9. An excellent match has been found between the theory and experiment within a porosity range of 40 to 70%. The mismatch beyond 70% porosity has been discussed elsewhere [12].

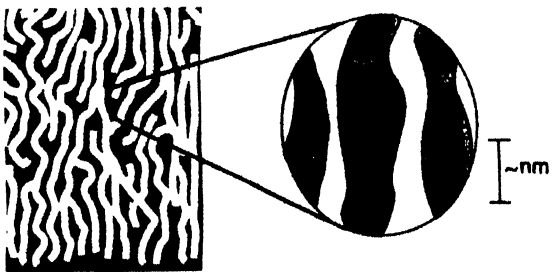

Figure 8. Ideal representation of a PS layer (left) the etched array of voids in Si, (right) an enlarged area of the PS layer where the Si-nano crystals are embedded in an amorphous oxide matrix (adopted from [18])

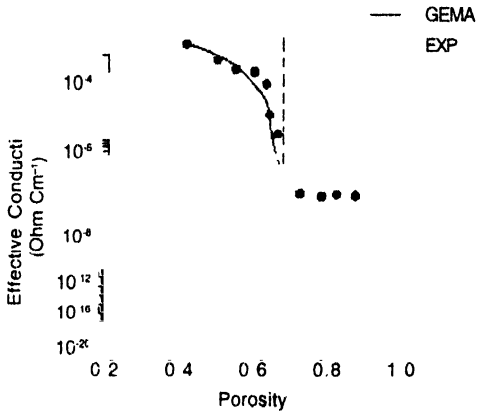

Figure 9. Comparison between calculated and experimental effective conductivity of PS

5. Vapour sensing principle

The working principle of a PS based capacitive vapour sensor is straightforward : vapour molecules are adsorbed from the environment into the porous layer and then diffuse into it. Due to the differences in permittivity, the capacitance of the layer changes as a function of the vapour uptake, which is directly related to the ambient vapour concentration [20,21]. The sensitivity of PS layer to the vapour is due to the adsorption of vapour molecules on its surface as well as condensation inside the pores. Thus, the adsorption-diffusion condensation kinetics of the vapour molecules inside the porous bulk and consequently the change in dielectric constant of the porous layer has been modeled with an effective medium approximation (EMA) [19–21].

When the transducer is placed in an environment with a certain vapour concentration level, the vapour molecules will be adsorbed at the surface of the porous layer. The rate of adsorption will be proportional to the ambient vapour concentration as well as to the exposed area of the porous layer for adsorption.

After adsorption, the vapour molecules will diffuse into the pores of the porous bulk until an equilibrium vapour content inside the porous dielectric is reached. This equilibrium vapour content will depend on the degree of void filling, which is again a function of the ambient vapour concentration level and the morphology of the porous dielectric. Due to this diffusion, the water vapour concentration at different layers of the porous dielectric will increase with time. The equilibrium vapour content depends on the degree of void filling, which is a function of the ambient humidity level and the morphology of the porous dielectric. Condensation of water vapour inside a porous dielectric takes place in all pores with a radius smaller than the Kelvin radius [20,22]. For cylindrical pores, which are closed at one end, the Kelvin radius is given by

$$r_k = -\frac{2\gamma M_v \cos\theta}{\rho_v RT \ln \frac{p_v}{p_s}} \tag{3}$$

where M_v, ρ_v and γ are the molecular weight, density and surface tension of the adsorbed vapour in liquid phase respectively, θ is the contact angle. p_v and p_s are the instantaneous and saturation vapour pressure inside the pore.

PS, with a certain equilibrium vapour content constitutes a random mixture of (oxidized) silicon, adsorbed, and condensed vapour and air. A capacitor with a porous dielectric consequently shows an as-measured or effective value directly proportional to the effective dielectric constant of the mixture. This is done in generalized effective medium approximations (GEMA). This GEMA describes effective dielectric constant (ε_{eff}) of an n-phase mixture of dispersed particles as

$$\frac{\varepsilon_i^{1/t} - \varepsilon_m^{1/t}}{\varepsilon_i^{1/t} + \frac{\psi_p}{1-\phi_p}\varepsilon_m^{1/t}} = 0 \tag{4}$$

where ε_i is the permittivity of the i-th phase with volume fraction v_i and ϕ_p is the percolation volume fraction.

The above equations enable us to compute the effective value of the dielectric constant of the porous layer with a certain amount of vapour content. Moreover, for a particular vapour type, one can compute the transient increase of the effective dielectric constant and thus predict the response time and sensitivity of the sensor both depending on the morphology of PS structure.

Treating the as-prepared PS as host material and the condensed vapour as the dispersed phase, the vapour sensitivity of the sensor (S) can be expressed as [23],

$$S = \frac{\varepsilon_{ps}(C_{\max}) - \varepsilon_{ps}(C_{\min})}{\varepsilon_{ps}(C_{\min})}. \tag{5}$$

5.1. PS vapour sensor :

Figure 10 shows the photograph of the vapour sensor in consideration. PS adsorbing layer was formed on the top surface by usual anodic etching method with graphite electrode and 1 : 1 HF-CH_3OH electrolyte. The planar uniformity of the PS surface depends on the surface roughness and on the distribution of the applied electric field lines [8], *i.e.*, the uniformity of the current density during PS formation. To reduce the effect of variation of surface roughness, polished wafers have been used for the preparation of PS layers. Further, instead of a single PS absorbing layer, small PS areas are fabricated and these small area PS capacitors are connected in parallel. The formation current density was ~20 mA/cm^2 for a 24% electrolytic bath to achieve the optimum porosity range of 65–75% for these samples. The PS layers are oxidized by immersing in boiling H_2O_2 for increased stability of the sensor. This oxidation helps to increase the stability of the sample so that further oxidation under exposure to humid ambient is slowed down considerably [15]. It also makes the PS layer more hydrophilic. Top metal contacts and micro heater were developed by vacuum evaporation of Al metal through a patterned shadow mask developed by standard photolithography technique. For establishment of ohmic contacts between PS layer and top electrodes, the sensor was annealed in N_2 atmosphere [12].

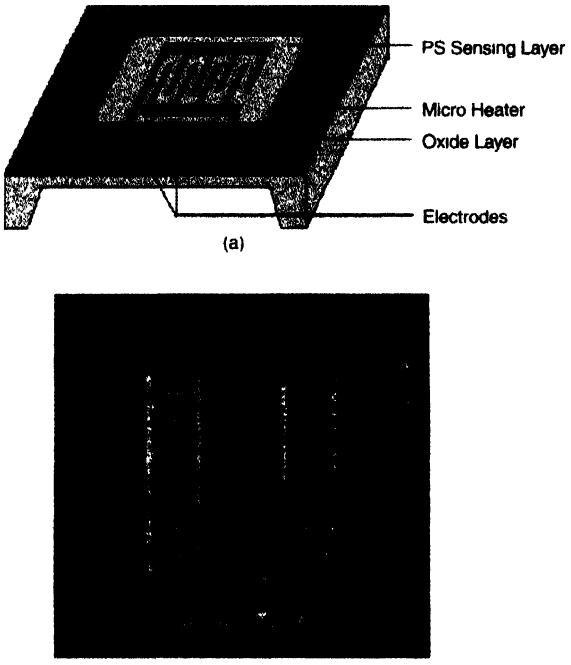

Figure 10. (a) Schematic and (b) actual structure of the PS vapour sensor

Figure 11 shows the transient behavior of a typical PS vapour sensor. The ambient water vapour concentration of the sensor was changed rapidly using experimental setup (15% rh, 25°C to 95% rh, 25°C). The sensor reacts within seconds, however, takes another few seconds to reach a stable value. Figure 12 shows vapour concentration *vs* scaled and linearized output voltage

from the developed vapour sensor for both increasing and decreasing vapour concentration. The figure shows a negligible hysteresis.

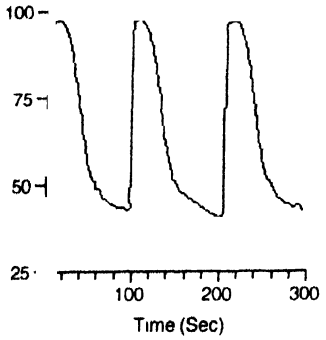

Figure 11. Transient characteristics of the PS vapour sensor

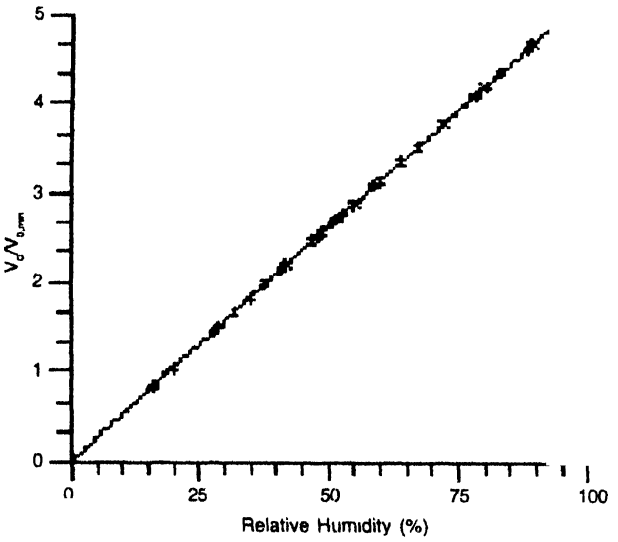

Figure 12. Relative sensitivity and linearity of the PS vapour sensor.

6. Electroluminescence in PS

The luminescence property of PS can also be realized by application of proper bias to the material. If a Schottky or p-n junction is formed with porous silicon and carriers are injected under forward biasing it emits visible electroluminescence (EL) as shown in Figure 13. The basic mechanism of EL is like PL under UV photoexcitation but here the excitation is made by

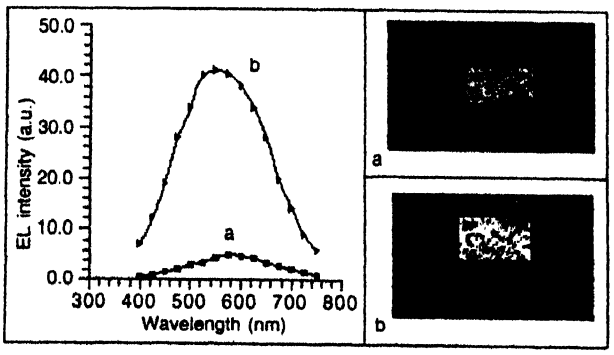

Figure 13. EL spectra and photograph of (a) Ag/PS Schottky LED and (b) p-n junction PS LED.

application of proper voltage across the junction. Probable transition processes during EL in oxidized PS is shown in Figure 14 and has been discussed in [24,25].

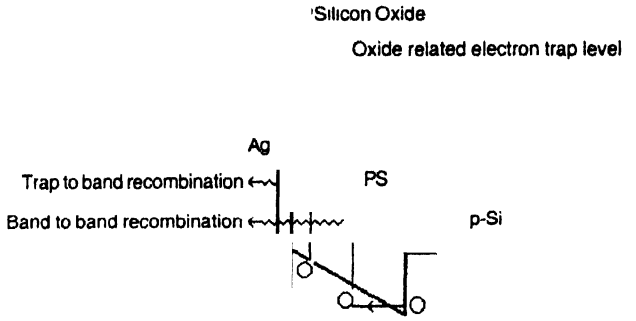

Figure 14. Schematic band structure and probable EL mechanism of Ag/PS/p-Si LED.

The external quantum efficiency of EL and peak wavelength are strongly dependent on the degree of quantum confinement within the Si-nanoparticles [26–28]. So with increasing porosity quantum efficiency of EL increases but this increase in porosity causes a strong decrease in conductivity (Figure 9) of the layer that hinders sufficient carrier injection from the external source leading to lowering in power efficiency of the PS LEDs. Figure 15 (a) and (b) show the variation of EL spectra and power efficiency of some PS LEDs fabricated by deposition of semi-transparent thin Ag film on PS layers prepared with different values of current density.

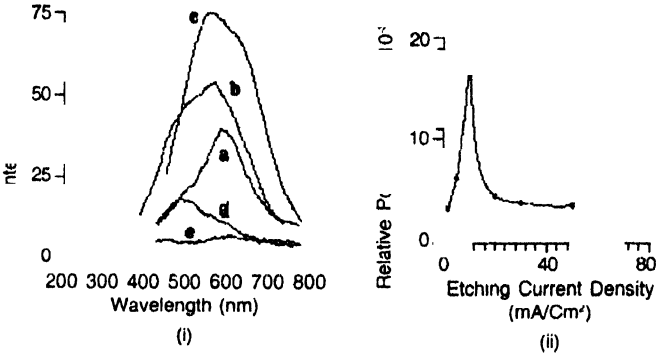

Figure 15. (i) EL spectra of PS Schottky diodes prepared with 24% HF for 2 min using the following current densities . (a) 2, (b) 5, (c) 10, (d) 30, (e) 50 mA/cm^2. (ii) Variation of relative power efficiency of PS Schottky LED with formation current density of the PS layer.

6.1. PS seven segment display :

For fabrication of seven-segment PS display device, a p-type (100) silicon wafer (ρ ~ 1–2Ω cm) has been taken. Thick silicon oxide (~1 μm) has been formed on the whole wafer front area. Black ink has been screen printed on the oxidized wafer for selective etching of oxide in 10% HF solution to design a seven-segment. After the selective etching of oxide, the black ink has been removed by treating it in TCE using an ultra sonic cleaner. This wafer then has been transferred to a diffusion furnace for boron doping. After obtaining a thick p^+ boron doped (~2 μm), n^+ diffusion (~1 μm) has been performed on the same wafer to

get n^+p^+ layer. Back ohmic contact has been established by screen printing of Ag-Al paste and its subsequent firing proper alignment of screen has been done to screen print black ink on the wafer for prevention of oxide layer. After baking of this black ink, porous silicon has been formed on the n^+p^+ diffused area through electrochemical etching process performed with proper electrode with guard ring for the sake of lateral uniformity of the layer. The etching current density and time was 10 mA/cm^2 and 3 minutes respectively. The HF concentration in the electrolyte was 24%. After the formation of PS layer, the wafer has been cleaned thoroughly with DI water and dried under clean air atmosphere and then it was transferred to a vacuum evaporation chamber for deposition of thin (~30 nm) Ag film. The black ink was then removed from the wafer. Standard photolithography has been employed to develop shadow mask on the wafer for evaporation of thick metal film to form the double layer grid structure [29] and the carrier collection contacts. Figure 16 shows the EL emission from the display. The length and width of each segment was 2 cm and 0.5 cm respectively.

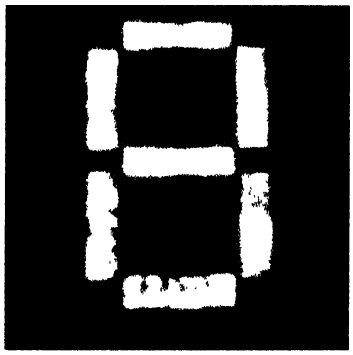

Figure 16. Photograph of light emission from the PS seven-segment display

7. Conclusions

Porous silicon is a naturally formed three-phase mixture of silicon nano crystallites, the embedded SiO_2 and the adjacent voids. The dimensions and morphology of porous silicon can be modulated significantly to result in silicon nano crystallites from tens of nanometers to a few nanometers by controlling the anodic formation parameters. Strong PL and EL are observed when the silicon nano crystallites have the dimensions in the range of a few nanometers (<5 nm). A band structure of oxidized PS having a fixed oxide trapping level explains most of the observed PL and EL behaviour of PS. A seven segment PS LED has been fabricated using double metallization technique.

Porous silicon is intrinsically an excellent sensing material, particularly for vapour sensing. The adsorbed-diffused-condensed vapour results into a significant change in its dielectric constant that can be used for highly sensitive capacitive sensing. The speed of response and sensitivity again depend to a large extent on the morphology and dimensions of porous silicon nano structures.

Acknowledgment

The authors wish to acknowledge the cooperation received from Dr. S K Dutta, Department of Physics, City College, Kolkata and Mr. S Banerjee, Department of Physics, Jadavpur University. One of the authors (SMH) acknowledge the financial support received from MNES, Government of India

References

[1] A Uhlir *Bell Syst Tech J.* **35** 333 (1956)

[2] L T Canham *Appl Phys Lett* **57** 1046 (1990)

[3] P M Fauchet (ed.) *IEEE J Select Topics Quantum Electronics* **4** 1020 (1998)

[4] Z Gaburro, P Bellutti and L Pavesi *Phys. Stat. Sol* **(a)182** 407 (2000)

[5] H Sinoda *et al. Nature* **400** 853 (1999)

[6] S Strehkle *et al. Solar Energy Mater Solar Cells* **58** 399 (1999)

[7] H Saha, S K Dutta, S M Hossain, S Chakraborty and A Saha *Bull. Mater Sci* **21** 195 (1998)

[8] S M Hossain, J Das, S Chakraborty, S K Dutta and H Saha *Semicond Sci. Technol.* **17** 55 (2002)

[9] G Amato *Jpn. J. Appl Phys* **34** 1716 (1995)

[10] M V Wolkin *et al Phys. Rev Lett* **82** 197 (1999)

[11] B D Cullity *Elements of X-ray Diffraction*, (2nd edn) Addison-Wesley

[12] S K Dutta, S M Hossain, S Chakraborty and H Saha *Phys Stat Sol (a)* **191** 535 (2002)

[13] Y M Niquet *et al. Phys Rev* **B62** 5109 (2000)

[14] H W Lau, G J Parker and R Greef *Thin Solid Films* **276** 29 (1996)

[15] S M Hossain, S Chakraborty, S K Dutta, J Das and H Saha *J Luminesc* **91** 195 (2000)

[16] G C John and V A Singh *Phys Rev* **B50** 5329 (1994)

[17] P Bettotti, M Cazzanelli, L Dal Negro, B Danese, Z Gaburro, C J Oton, G Vijaya Prakash and L Pavesi *J Phys.. Condens Matter* **14** 8253 (2002)

[18] L Pavesi and R Guardini *Brazillian J Phys* **26** 151 (1996)

[19] D S McLachlan *Solid State Commun* **72** 831 (1989)

[20] Z M Rittersma and W Benecke *Sensors and Materials* **12** 35 (2000)

[21] J Das, S M Hossain, S Chakraborty and H Saha *Sensors and Actuators* **A94** 44 (2001)

[22] G M O'Halloran, M Kuhl, P J Trimp and P J French *Sensors and Actuators* **A61** 415 (1997)

[23] H Saha, J Das and S M Hossain *Asian J Phys.* (Accepted for publication) (2003)

[24] P M Fauchet, N Koshida and S R J Brueck *Advanced Luminescent Materials* (ed). Lockwood, (Pennington : The Electrochemical Society) (1996)

[25] D Dimova Malinpvska *Thin Materials and Devices-Developments in Science and Technology*, (eds) J M Marshall, N Kiorov, A Vavarek and J M Maud (Singapore . World Scientific) p.58 (1999)

[26] M S Hybertsen *Phys Rev Lett.* **72** 1514 (1994)

[27] M S Hybertsen in *Porous Silicon Science and Technology* (eds.) J C Vial and J Derrien (Les Editions de Physique, Les Ulis, France), **1** 67 (1995)

[28] M S Hybertsen in *Light Emission from Silicon* (eds) S S Iyer, R T Collins and L T Canham (Materials Research Society, Pittsburgh, Pennsylvania) **256** 179 (1992)

[29] S M Hossain, S Chakraborty, S K Dutta and H Saha *Microelectronic Engineering* **56** 303 (2001)